The effect of density on the inherent structure in liquids

Thomas A. Weber and Frank H. Stillinger
Bell Laboratories, Murray Hill, New Jersey 07974

(Received 5 October 1983; accepted 9 December 1983)

We have previously shown that diffusion and fluid flow within a liquid may be interpreted as transitions between mechanically stable arrangements of the molecules, i.e., local minima in the potential energy for the system as a whole. In addition, our previous work has shown that the equilibrium thermodynamic properties of the liquid and solid can be rigorously and usefully explained in terms of vibrational excitations within, and shifting equilibrium between, these stable molecular packings. Previously, we have determined transition rates between various packings as a function of temperature, system size, and extent of supercooling. In the present work, we study the effect of density on both the number and distribution of packing structures. Molecular dynamics simulations were carried out for systems of 32 and 108 argon-like particles at three densities. The primary observations and conclusions are: (1) as the density decreases the total number of different amorphous packing structures increases; (2) the density at which the amorphous material has its minimal average energy is about 3% lower than the density at which the crystalline material has its minimal energy; (3) the activation energy to self-diffusion is found to increase with increasing density.

I. INTRODUCTION

In a series of recent papers[1–4] we have advanced a new approach to understanding the liquid state and the melting process by separating the statistical mechanics problem of constructing a partition function into two parts. In the first instance we focus on all of the inherent mechanically stable packing configurations. In the second instance we account for the vibrational motion, usually anharmonic, about these stable points. In the previous work,[4] we looked at both the static properties such as different packing structures and also looked at the transitions between regions belonging to different stable configurations. In the present work, we study the effect of density variation on the packing structures and dynamical properties.

An N particle system in D dimensions subject to periodic boundary conditions has a configuration at any time t represented by a DN-dimensional vector $\mathbf{r}(t)$. If the potential energy of interaction is given by $\Phi(\mathbf{r})$, assumed to be differentiable, then the stable packing configurations are a subset of the solutions to

$$\nabla\Phi(\mathbf{r}) = 0. \tag{1.1}$$

The lowest energy solution of Eq. (1.1) yields the stable packing configuration of maximal crystallinity. Other solutions of Eq. (1.1) yield packing configurations which are relative minima.

All of configuration space, with the exception of a few configurations of vanishing measure, may be uniquely assigned to a particular Φ minimum by a steepest-descent "quench" connection. As the Newtonian equations of motion evolve in time, $\mathbf{r}(t)$ would in principle quench to a sequence of different packing configurations presuming that the system has sufficient energy to traverse the barriers separating the regions belonging to the various minima.

One expects[4] that the number of local minima Ω for large N will vary with N as follows:

$$\Omega \approx N!\exp(\nu N). \tag{1.2}$$

The first factor accounts for all the possible permutations of particles within a given configuration which yield identical energies. The second factor estimates the number of distinct ways of arranging stable packings. Rough estimates for ν as a function of density are provided below for our model potential.

In Sec. II we discuss the simple model potential used in the present study and also the numerical techniques used to generate both the trajectories and the quench configurations. In Sec. III the equation of state for the system at three reduced densities $\rho = 0.9$, 1.0, and 1.1 is presented. In addition radial distribution functions, hereafter rdf's, are shown for both the crystal and the fluid.

Section IV details the effect of density on the different packing states and shows the dramatic way in which both the number and distribution of the amorphous configurations change with density. Section V discusses the effect of density upon the self-diffusion of particles. The final Sec. VI summarizes the conclusions and points to directions for future work.

II. COMPUTATIONAL PROCEDURE

The Lennard-Jones 12-6 potential has been used extensively to simulate noble gases such as argon.[5–7] In reduced units this potential has the form

$$v_{LJ}(r) = 4(r^{-12} - r^{-6}), \tag{2.1}$$

which has the following properties:

$$\begin{aligned} &v_{LJ}(1) = 0, \\ &v_{LJ}(2^{1/6}) = -1, \\ &v'_{LJ}(2^{1/6}) = 0. \end{aligned} \tag{2.2}$$

A numerical disadvantage of the Lennard-Jones potential is that the interactions only go to zero at infinity; it has become frequent practice to use a potential cutoff which ignores all contributions beyond some fixed distance. The choice of this cutoff distance is arbitrary, but produces discontinuities in

 0021-9606/84/062742-05$02.10

time derivatives of the forces. Instead of using such an arbitrary cutoff we have chosen a potential of the form

$$v(r) = A\,[r^{-p} - r^{-q}] \exp\,[(r-a)^{-1}] \quad (0<r<a)$$
$$= 0 \qquad\qquad\qquad\qquad\quad (a \leqslant r) \qquad (2.3)$$

This potential automatically satisfies the first equation of Eq. (2.2) and can be made to satisfy the other two equations by an appropriate choice of A and a. In addition $v(r)$ and all of its derivatives go to zero at a. When $p = 12$ and $q \to 6-$, $v(r)$ of Eq. (2.3) becomes the 12-6 Lennard-Jones potential. In the present study, $p = 12$ and $q = 0$ which determines the values of $A = 8.805\,977$ and of $a = 1.652\,194$. All force derivatives relevant to the dynamics are rendered continuous by the form (2.3)

Molecular dynamics studies of the melting of perfect face-centered cubic crystals were performed at three reduced densities $\rho = 0.9$, 1.0, and 1.1. The melting was accomplished by heating perfect crystals which had the normal periodic boundary conditions with $4n^3$ particles in the basic cubical cell. Some simulations were performed using 32 particle cells which allowed the direct counting of all (or nearly all) packing structures while the majority of computations were performed using 108 particle systems. The classical equations of motion were integrated using a fifth-order Gear algorithm.[8]

The simulations were carried out in reduced units where particle mass was unity, and where the depth and range of $v(r)$ as shown in Eqs. (2.2)–(2.3) fix the units of energy and distance. Comparison to argon properties may be made by recalling that the unit of distance for that substance is 3.4 Å and the unit of energy is 120 K. The integration time step was

$$\Delta t = 0.001\,25, \qquad (2.4)$$

which corresponds to 2.7×10^{-3} ps for Ar. After the system was heated or cooled to a new temperature by uniformly scaling the momenta, relaxation runs of at least $2 \times 10^3\ \Delta t$ were performed. Runs of at least $10^4\ \Delta t$ were carried out to measure properties such as diffusion constants, average potential energy, and radial distribution functions. In order to study the inherent packing structures which underlie the liquid at time t in a given trajectory, the instantaneous system configuration $\mathbf{r}(t)$ is quenched (typically every ten Δt) to locate the relevant minimum. This quenching operation requires extensive amounts of computer time and is executed using a combination of a conjugate-gradient and a quasi-Newton method.[9] For the 32 particle system it is possible to estimate the number of distinct minimum energy states for all three densities. Since the number of states grows exponentially with system size, the overwhelming numbers of distinct potential minima which exist for $N = 108$ can at best only be sampled in a representative rather than an exhaustive manner.

III. EQUATION OF STATE

The potential energy per particle is given by

$$\phi \equiv N^{-1}\Phi = N^{-1}\sum_{i<j} v(r_{ij}). \qquad (3.1)$$

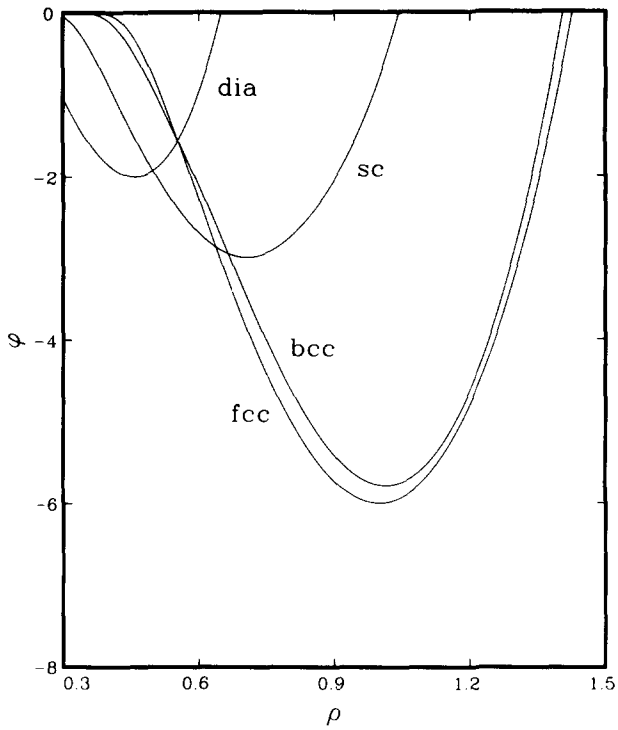

FIG. 1. Lattice energies per particle for the diamond, simple cubic, face-centered cubic, and body-centered cubic lattices as a function of density.

This energy as a function of density is shown in Fig. 1 for the diamond, simple cubic, body-centered cubic, and face-centered cubic lattices. The hexagonal close-packed lattice has an energy nearly identical to that of the fcc lattice in the density range shown on the plots. Above a density of $\rho = 0.64$ the fcc lattice is found to be the lattice with minimum energy. The absolute minimum in energy is found to occur at a density near $\rho = 1.0$. The energy for the fcc lattice at the three densities $\rho = 0.9$, 1.0, 1.1 are listed in Table I as $\Phi_{\min}$.

The pressure as a function of temperature determined by the molecular dynamics simulation is shown in Fig. 2 for the three densities. Pressure is determined from the virial equation

$$P = \frac{1}{V}\left\{(N-1)T + \frac{1}{3}\sum_i \overline{\mathbf{F}_i \cdot \mathbf{r}_i}\right\}, \qquad (3.2)$$

where $\mathbf{F}_i$ is the force on the ith particle and $\mathbf{r}_i$ is its position. A factor of $N-1$ is used because the center of mass is held fixed. A pressure of 10 in our reduced units corresponds to 4.2 kbar for Ar.

TABLE I. System properties vs density.

ρ	0.9	1.0	1.1
$\phi_{\min}$	− 5.729 292 00	− 6.000 005 22	− 5.707 284 42
T_m	1.2	1.9	2.8
$\Omega_{32}/32!$	629	146	52
ν	0.20	0.16	0.12
ϕ_D	− 5.218	− 5.349	− 4.862
$\Delta\phi_{\text{melt}}/T_m$	0.463	0.466	0.463
A_d	0.060 66	0.073 87	0.046 04
ΔE_d	2.341 3	4.126 1	4.751 8

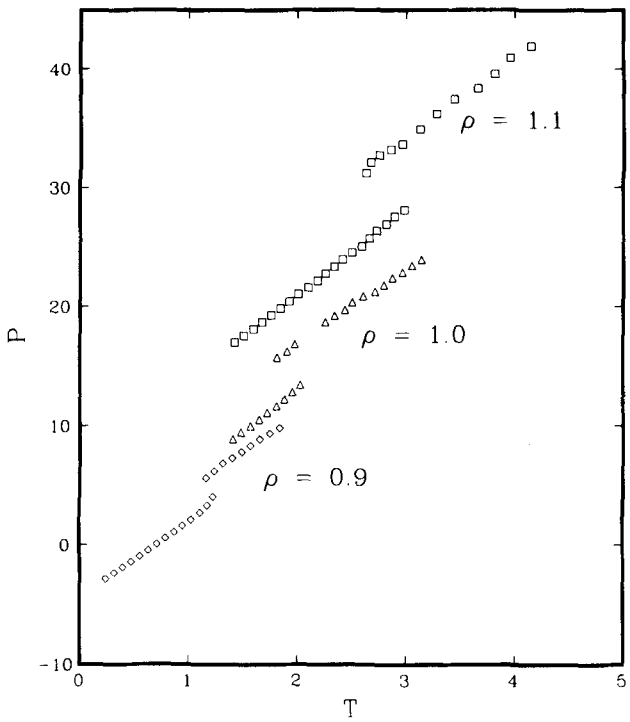

FIG. 2. Pressure vs temperature melting curves for three densities. All runs were made with 108 particles starting from the perfect fcc lattice at $T = 0$.

The melting temperature T_m is estimated from the break in the curve of pressure vs temperature. Table I lists the melting temperature for the three densities studied.

From a plot of the potential energy per particle vs temperature the latent heat of melting may be estimated. The liquid and solid branches of the melting curve were fitted with straight lines using linear least squares. Points in the coexistence region of the curves are excluded from the fits. The difference of these two functions each evaluated at the melting point yields the approximate latent heat of melting $\Delta\phi_{\text{melt}}$, which is found to go as

$$\Delta\phi_{\text{melt}} \approx 0.46 T_m .$$

Figure 3 shows the radial distribution functions of the unmelted crystal at $T \approx 0.8 T_m$ for the three densities studied. The first peak of the rdf corresponds to the 12 nearest neighbors of the fcc lattice. The second peak at ~ 1.6 corresponds to the six second neighbors. The third peak corresponding to the 24 third neighbors appears at a distance just below 2. Figure 4 shows the rdf's of the liquid at $T \approx 1.4 T_m$ for the three different densities. Notice that the maxima of both the first and second peaks shift to larger r values as ρ decreases, as would be expected.

IV. DENSITY OF STATES

When the system is at low temperatures prior to melting, a quench of any configuration at any time during the trajectory invariably reproduces the perfect fcc lattice. That is, the quenching simply removes phonon displacements. However once melting has occurred, quenches at various times along the trajectory will produce a diverse set of different energies each corresponding to different stable but noncrystalline arrangements of particles. Previously[4] we attempted to enumerate all such stable configurations for the

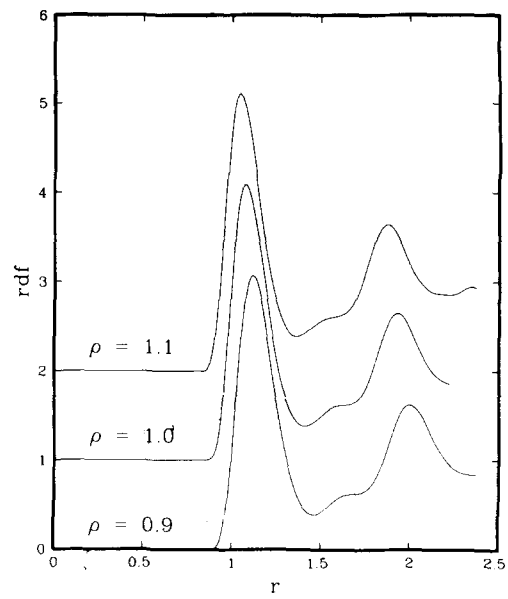

FIG. 3. Radial distribution functions for crystal structures ($T \sim 0.8\ T_m$) at three densities.

32 particle system at density $\rho = 1.0$ by cataloging all of the distinct quench energies produced in a series of runs of 10^4 steps each created at 13 different temperatures in the fluid. In this manner 157 distinct stable packings were discovered. Most of the higher energy, less stable configurations (i.e., those configurations of far less than optimal packing geometries) were only discovered in the higher temperature runs and were found to have a very low probability of occurrence.

To map out the most important stable packing configurations for the 32 particle systems at the three densities of present interest a consistent and identical approach was used for each. Trajectories of 3×10^4 steps were produced at each density with quenching every 10 time steps. The nominal

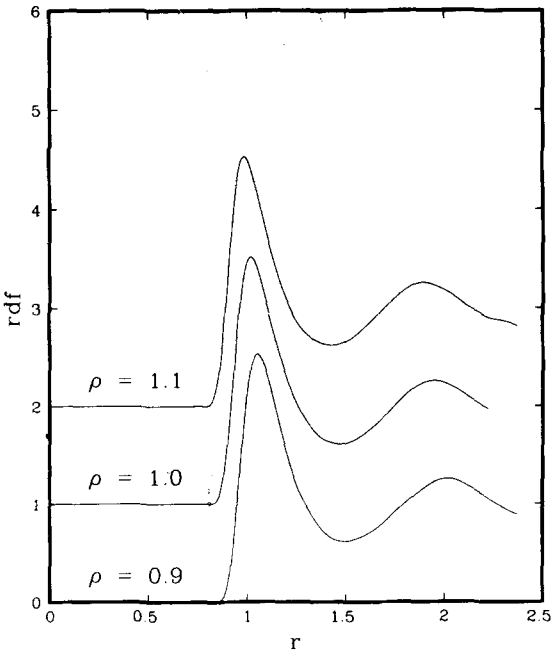

FIG. 4. Radial distribution functions for the liquid ($T \sim 1.4\ T_m$) at three densities.

reduced temperature for each density was approximately 6.5, well above T_m. The number of stable packing states identified in this manner was found to depend dramatically on density:

$$\Omega_{32}/32! = \begin{cases} 659 \\ 146 \\ 52 \end{cases} \text{ for } \rho = \begin{cases} 0.9 \\ 1.0. \\ 1.1 \end{cases} \tag{4.1}$$

A comparison of the state energies generated in the current study with our previous enumeration[4] shows that the discrepancy in the $\rho = 1.0$ determination is due to a failure in the present restricted study to discover some of the higher energy, less probable packings. A more accurate cataloging could be accomplished by running much longer trajectories; however the few extra states that would be so discovered would not justify the added expense. In addition since each density is treated in the same manner this would almost certainly not affect the conclusions regarding the dramatic density dependence. The ν parameter of Eq. (1.2) is found to vary with ρ, thus,

$$\nu = 0.16 + 4.0(1.0 - \rho) \tag{4.2}$$

over the density range studied, where the two significant figures given are consistent with our counting accuracy.

As the system size is increased from 32 to 108 particles it becomes obviously impossible to determine all the stable packing structures. Even at the highest density where 52 states were found for the 32 particle system, approximately 0.5×10^6 distinct states are expected for the 108 particle system. Figure 5 shows quench energy trajectory plots for 108 particle runs for the three densities at $T \sim 6.5$. Each run is 10^4 time steps with quenching every ten time steps. Even at the elevated temperature of the runs it is evident that quenches to the lowest energy crystal structure are found. The gap between the crystal state and the first state in the excited (amorphous) manifold, and also the width of the distribution, both decrease with decreasing density.

Figure 6 shows the distribution of different states in the 108-particle system as a function of potential energy for the three densities. The energy per particle of the low energy crystal state $\Phi_{\min}$ and of the most probable energy state in the amorphous manifold ϕ_D (the maximum of the distribution) are listed in the table.

The amorphous-state, distribution-maximum energy ϕ_D is found by quadratic interpolation to have its minimum value at a density of 0.97. This amounts to a 3% shift in density between the most stable crystal structure ($\rho \cong 1.0$) and the amorphous packings ($\rho \cong 0.97$). Thus at constant pressure the amorphous state would be less dense than the perfect crystal.

V. SELF-DIFFUSION

Recently Zwanzig[10] has developed a theory to predict the relationship between the self-diffusion constant of a liquid and its shear viscosity. Just as in the present work, in that theory the liquid is pictured as (instantaneously) localized near and vibrating around the potential minimum associated with a specific packing structure. After a certain time, specified by a jump frequency, the system makes a transition to another region and vibrates around this new packing minimum. Within one such region the oscillations are described by the Debye approximation and thus are characterized by the longitudinal and transverse sound velocities.

In our study we have undertaken the direct measurement of the self-diffusion constant as a function of both temperature and density. The self-diffusion constant is given by the well-known Einstein relationship

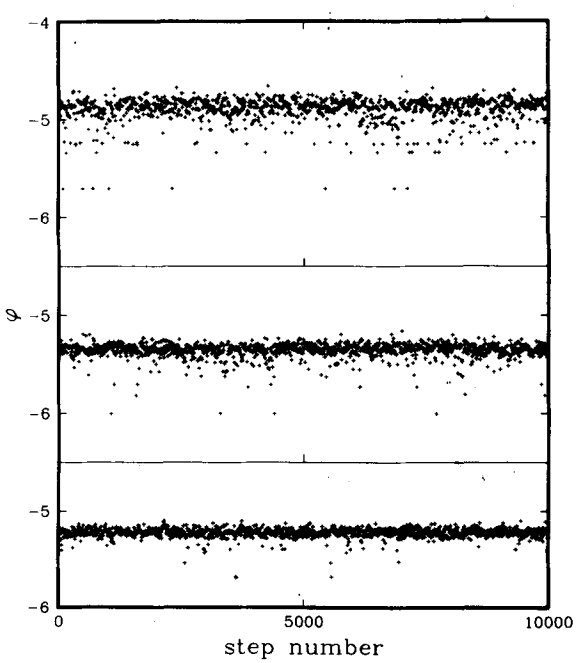

FIG. 5. Trajectory plots of the quench energy per particle for runs at $T \sim 6.5$. The density is $\rho = 0.9$ for the lower plot, $\rho = 1.0$ for the middle plot, and $\rho = 1.1$ for the upper plot.

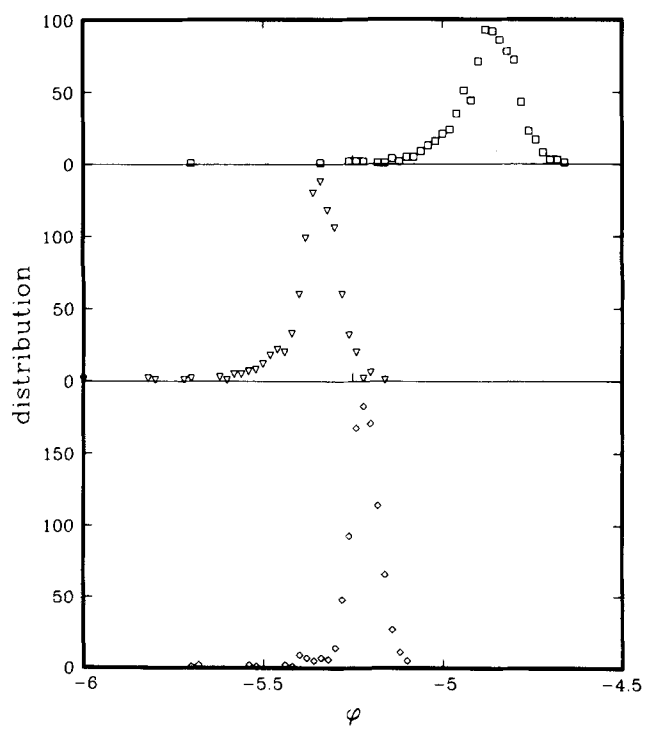

FIG. 6. Quench energy distribution functions for the runs at $T \sim 6.5$. The lowest curve refers to $\rho = 0.9$, while the uppermost curve is the $\rho = 1.1$ plot.

$$D = \lim_{t\to\infty} \frac{1}{6tN} \langle |\mathbf{r}(t) - \mathbf{r}(0)|^2 \rangle, \tag{5.1}$$

where $\mathbf{r}(t)$ is the configuration of all N particles of the fluid at time t. Figure 7 shows the measured self-diffusion constants for various temperatures and densities. These quantities have been determined by linear least-squares fits of the mean-squared displacement, $|\mathbf{r}(t) - \mathbf{r}(0)|^2$ from steps 2 500 to 10 000 for well-equilibrated runs. The scatter in the data is primarily due to the fact that only one trajectory was run at a given temperature to calculate the mean-squared displacement.

The self-diffusion constants were then fitted by least squares to

$$D = T^{1/2} A_D \exp[-\Delta E_D/T]. \tag{5.2}$$

The parameters A_D and ΔE_D are listed in Table I for the three densities. The straight lines in Fig. 7 show the best fit we have obtained to the self-diffusion constant data. In each case the line was plotted from the melting point for that density to a high temperature. The values of D obtained below the melting points were not used in the fits because the trajectories were probably not run long enough to determine self-diffusion constants accurately.

For the 32 particle system at density $\rho = 1.0$ we had found that the rate for making transitions from one amorphous packing to another varied with temperature approximately

$$KT^{1/2} \exp[-2.16/\mathrm{T}]. \tag{5.3}$$

The limited transition rate data available for the 108 particle system at $\rho = 1.0$ also fits on the same curve after appropriately scaling the prefactor K. The activation energy for self-diffusion however is nearly twice that for transition between amorphous packing structures: 4.13 compared with 2.16.

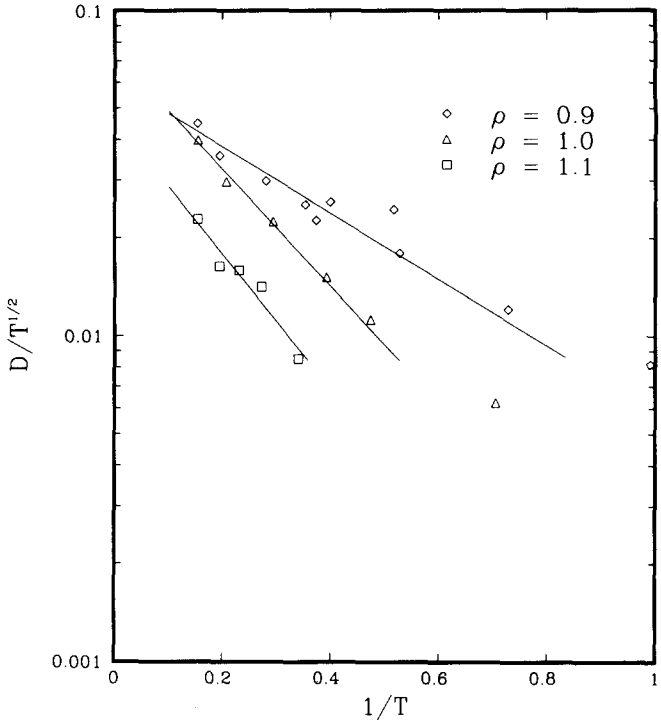

FIG. 7. Self-diffusion constant plots as a function of temperature. The open figures are the simulation data as determined from the mean-squared displacement. The solid lines are the best fit to the data using Eq. (5.2).

VI. DISCUSSION

As shown in this work the number and distribution of amorphous packing structures strongly depends on density. As the density increases the number of available states decreases. In addition the particle mobility as measured by the self-diffusion constant is observed to decrease. The activation energy for particle self-diffusion increases with increasing density.

The amorphous packing structures are found to have their minimum energy, as measured by ϕ_D, at a lower density than the maximal crystal packings. Thus the amorphous structures are inherently less dense than the crystalline structures.

At each density the distribution of packing states is asymmetrically skewed toward lower energy. The total number of available states within the amorphous manifold increases dramatically as the density is decreased. In addition the width of the distribution decreases with decreasing density, implying that less energy is required to incorporate defect structures at the lower density.

The activation energy for self-diffusion has been found to increase with increasing density. However this activation energy may not be attributed solely to the activation energy required to move from one packing configuration to another since they differ roughly by a factor of 2.

A natural extension of the work reported here would focus on those other solutions to Eq. (1.1) which are saddle points of Φ. These other extrema need to be carefully characterized both as to their height above flanking minima and as to curvatures of Φ. Such information is vital to understanding transition rates along the lines established by absolute reaction rate theory in chemical dynamics.[11] It would also help to elaborate substantially the Zwanzig view of flow in liquids mentioned earlier.

[1]F. H. Stillinger and T. A. Weber, Kinam A **3**, 159 (1981).
[2]F. H. Stillinger and T. A. Weber, Phys. Rev. A **25**, 978 (1982).
[3]F. H. Stillinger and T. A. Weber, J. Phys. Chem. **87**, 2833 (1983).
[4]F. H. Stillinger and T. A. Weber, Phys. Rev. A **28**, 2408 (1983).
[5]A. Rahman, Phys. Rev. **136**, 405 (1964).
[6]A. Rahman, M. J. Mandell, and J. P. McTague, J. Chem. Phys. **64**, 1564 (1976).
[7]S. R. Nagel, A. Rahman, and G. S. Grest, Phys. Rev. Lett. **47**, 1665 (1981).
[8]C. W. Gear, Argonne National Lab. Rep. ANL-7126, January, 1966.
[9]R. Fletcher, *Practical Methods of Optimization* (Wiley, New York, 1980).
[10]R. Zwanzig, J. Chem. Phys. **79**, 4507 (1983).
[11]S. Glasstone, K. J. Laidler, and H. Eyring, *The Theory of Rate Processes* (McGraw-Hill, New York, 1941).